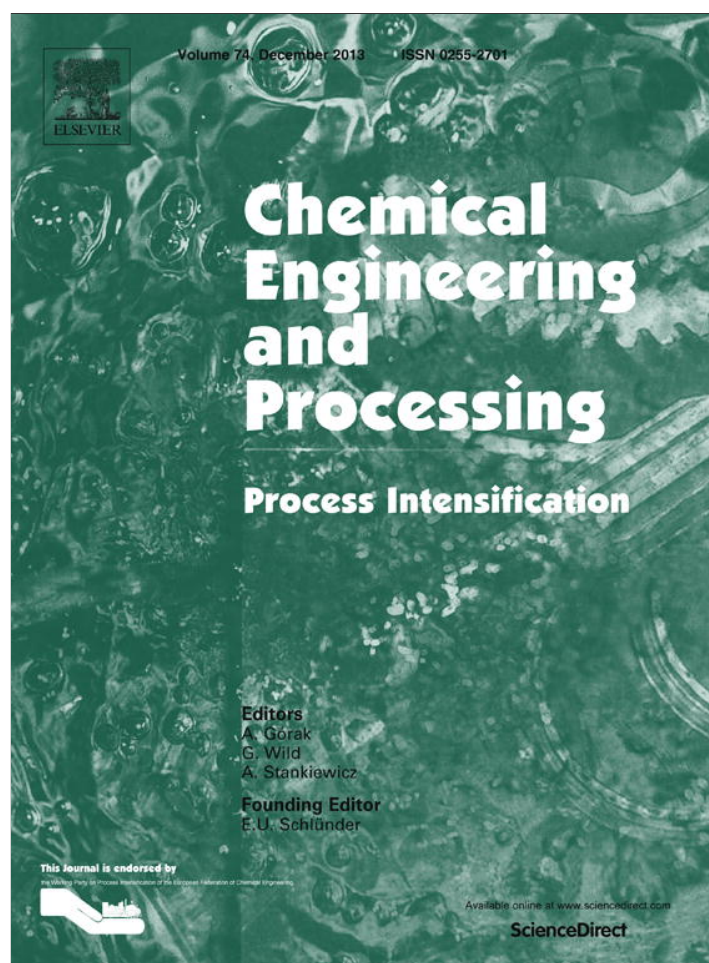


Provided for non-commercial research and education use.
Not for reproduction, distribution or commercial use.



This article appeared in a journal published by Elsevier. The attached copy is furnished to the author for internal non-commercial research and education use, including for instruction at the authors institution and sharing with colleagues.

Other uses, including reproduction and distribution, or selling or licensing copies, or posting to personal, institutional or third party websites are prohibited.

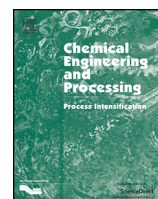
In most cases authors are permitted to post their version of the article (e.g. in Word or Tex form) to their personal website or institutional repository. Authors requiring further information regarding Elsevier's archiving and manuscript policies are encouraged to visit:

<http://www.elsevier.com/authorsrights>



Contents lists available at ScienceDirect

Chemical Engineering and Processing: Process Intensification

journal homepage: www.elsevier.com/locate/cep

Design, optimization and controllability of an alternative process based on extractive distillation for an ethane–carbon dioxide mixture



Carlo E. Torres-Ortega^a, Juan Gabriel Segovia-Hernández^{a,*}, Fernando I. Gómez-Castro^a, Salvador Hernández^a, Adrián Bonilla-Petriciolet^b, Ben-Guang Rong^c, Massimiliano Errico^d

^a Universidad de Guanajuato, Campus Guanajuato, Division de Ciencias Naturales y Exactas, Departamento de Ingeniería Química, Noria Alta S/N, Guanajuato, Gto. 36050, Mexico

^b Instituto Tecnológico de Aguascalientes, Departamento de Ingeniería Química, Av. Adolfo López Mateos #1801 Ote., Fracc. Bona Gens, C.P. 20256 Aguascalientes, Ags., Mexico

^c Institute of Chemical Engineering, Biotechnology and Environmental Technology, University of Southern Denmark, Niels Bohrs Allé 1, DK-5230 Odense M, Denmark

^d Università degli Studi di Cagliari, Dipartimento di Ingegneria Meccanica, Chimica e dei Materiali, Via Marengo 2, 09123 Cagliari, Italy

ARTICLE INFO

Article history:

Received 17 May 2013

Received in revised form

26 September 2013

Accepted 29 September 2013

Available online 23 October 2013

Keywords:

Extractive distillation

Optimization

Multi-objective differential evolution

Singular value decomposition

Thermodynamic efficiency

Greenhouse gases generation

ABSTRACT

Alternative configurations based on cryogenic extractive distillation were proposed and simulated by using Aspen Plus 7.0[®] coupled to a multi-objective stochastic optimization procedure (differential evolution, DE). The evaluation of the performances of the proposed configurations was focused on the ethane–carbon dioxide azeotrope separation considering different liquefied hydrocarbon fractions as entrainers. The design alternatives were compared to the conventional chemical absorption system.

The proposed sequences were simultaneously Pareto optimized by minimizing the total annual cost (TAC) and maximizing the acid gas removal. Complementary studies regarding the theoretical control properties, the thermodynamic efficiency and the greenhouse gases generation were conducted for several representative operating conditions obtained from the Pareto optimized fronts. The proposed cryogenic extractive distillation sequences realized the higher carbon dioxide removal together with the lower TAC compared to the conventional chemical absorption system.

© 2013 Elsevier B.V. All rights reserved.

1. Introduction

According to the BP Outlook [1] and due to the great abundance of the natural gas reservoirs, this fossil fuel will represent the 25% of the energy sources in 2030. It is clear that the optimization of the natural gas treatment process will be fundamental to use efficiently this energy source.

The whole natural gas treatment can be summarized in four steps: acid removal, dehydration, heavy component removal and liquefaction [2]. The gas sweetening is a separation process aimed to remove acid gases, like carbon dioxide and hydrogen sulfide, from the natural gas. The separation of these gases is essential to avoid some operational and safety drawbacks in the natural gas treatment as the reduction on the heat capacity of the gas, the solidification of CO₂ on the next cryogenic steps, the corrosive properties

(powered by the presence of water), the formation of by-products, the toxicity, etc.

The intensification of the sweetening section of the process has been studied by different researchers [3,4]. Moreover, the carbon dioxide removal has an extensive interest in other application fields related to the natural gas employment, like the power generation plants [5,6]. In addition to this, another relevant scheme for carbon dioxide separation, namely EOR (enhanced oil recovery), is used. In EOR, the carbon dioxide is utilized to extract the oil from the underground [7,8].

The carbon dioxide removal, from natural gas or other sources, is a long studied topic and among all the alternatives proposed, the absorption using aqueous solution of alcohol–amines is for sure the most widely used process. This configuration is reported in Fig. 1.

Fig. 2 shows a carbon dioxide separation flowsheet utilizing a cryogenic extractive distillation column where some of the natural gas liquid (NGL) is recycled as an entrainer.

Compare to the previous process, this alternative has some advantages:

* Corresponding author. Tel.: +52 473 732 0006x8142.

E-mail addresses: gsegovia@ugto.mx, g_segovia@hotmail.com (J.G. Segovia-Hernández).

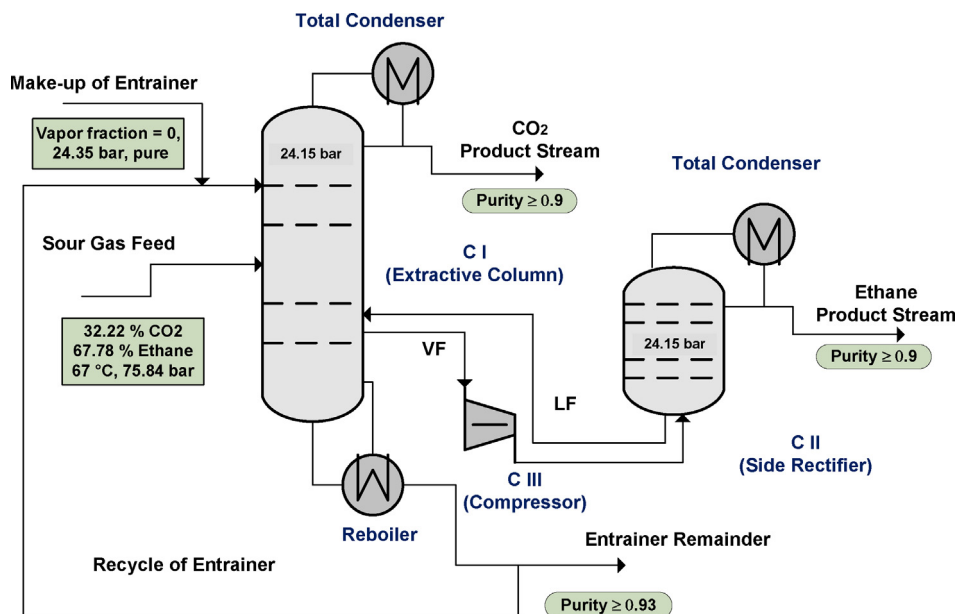


Fig. 3. Cryogenic extractive distillation with side rectifier (thermally coupled sequence by recycling some liquefied natural gas, CEDSR), molar basis.

The proposed thermally coupled sequence is derived from the extractive sequence reported in Fig. 2 by substitution of the extractive column's reboiler with a thermal coupling and moving the stripping section of the solvent recovery column below the thermal coupling location. The resulting configuration, reported in Fig. 3, represents an alternative thermally coupling distillation sequence for carbon dioxide removal. For all the cases the separation can be considered related to three components: ethane, carbon dioxide and the entrainer.

3. The alternative Petlyuk extractive sequence

The natural evolution of the thermally coupled sequence is the Petlyuk configuration, which can be considered, in some cases, equivalent to the divided wall column (DWC). The divided wall column was extensively studied for ternary mixtures or combined with simple columns [14–16].

With regard to the specific case of extractive distillation using a Petlyuk configuration, the implementation of this scheme is based on the use of a main column and a post-fractionator [17–19] as reported in Fig. 4. It can be noticed that the solvent and the sour gas are fed to the main column where carbon dioxide is obtained as distillate; the solvent is recovered from the bottom, while ethane is withdrawn as a side stream. The process analysis was focused on breaking the ethane–carbon dioxide azeotrope analyzing the conventional extractive distillation sequence and their derived thermally coupled configurations for different entrainers through the modeling of the sequences and the optimization of the designs. As a complementary analysis, the alternative configurations were compared with the conventional chemical absorption systems.

In this work, the Aspen Plus 7.0 process simulator is used to model those schemes, considering a rate based model.

4. Optimization procedure

4.1. Modeling of the separation process

To model the process, it is necessary to define a set of fundamental equations and correlations in order to correctly predict the studied phenomena. For the nature of the process analyzed in this study, this is formulated as a mixed integer non-linear

programming problem (MINLP) due to the coexistence of continuous and discrete design variables.

The non-equilibrium thermodynamic model has been used in different studies showing a good agreement with experimental data [20,21] and, for this reason, it was chosen in all the simulations performed in the present study. The non-equilibrium thermodynamic model, based on MERSHQ equations (i.e., mass balances, energy balance, rate of mass and heat transfer, summations of compositions, hydrodynamic equation of pressure drop and equilibrium relation), is characterized by high levels of non-linearity and, difficulties in the convergence, are common problems for the optimization task.

On the other hand, stochastic optimizers deal, in a robustly and efficiently way, with multi-modal and non-convex problems.

The default correlations in the non-equilibrium model (rate-based on Aspen Plus) implemented in the simulator like the mass transfer method of Chan and Fair [22], the Chilton–Colburn theory for the heat transfer [23] and for the interface area, as well as all the parameter for hydraulic calculations [24] were used.

For the prediction of the thermodynamic properties, two methods were chosen:

- Peng Robinson: for the alternative arrangements, it is suitable for non-polar or slightly polar mixtures at high temperature and pressure [25].
- Kent-Eisenberg method: that is used in the conventional chemical absorption. This method has been reported as one of the best in the prediction of aqueous system of amines with acid gases [26].

4.2. Definition of the optimizer used

Several heuristic techniques for global optimization mimicking biological evolution have been reported in the literature highlighting a new class of evolutionary methods called differential evolution (DE) algorithms. For different theoretical and practical problems, comparative studies have shown that the performance of DE-type algorithms are clearly better than those obtained for other stochastic algorithms [27,28].

In the present work the multi-objective differential evolution method developed by Sharma and Rangaiah [29] was applied to

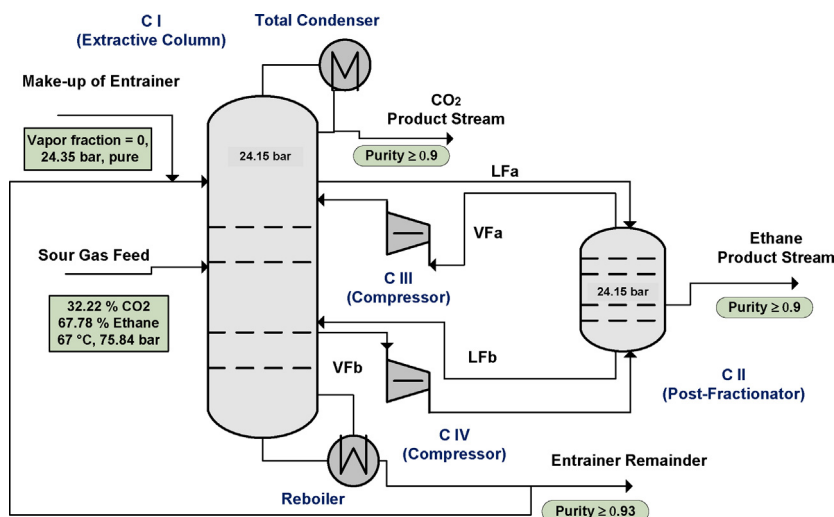


Fig. 4. Petlyuk cryogenic extractive distillation (thermally coupled sequence by recycling some liquefied natural gas, PCED), molar basis.

obtain the optimal design for the alternative sequences proposed. The main iterative steps of traditional DE are performed in each generation, for each target individual in the current population of N_p individuals and they include:

Mutation: random selection of three different vectors (individuals of the population) and generation of a mutant vector according to Eq. (1) (differentiation). The difference between the vectors (x_1 and x_2) defines the direction and length of the searching step. The vector x_3 represents a reference and F the mutation's factor that multiplies the difference of vectors. This difference will change along the optimization (i.e., the algorithm is self-adaptive).

$$x_{\text{mutant}} = x_3 + F(x_2 - x_1) \quad (1)$$

Crossover: creation of a trial vector by crossover of mutant and target individuals with a certain probability Cr .

Selection: either the target vector or the trial vector is chosen according to the best fitness for the next generation in order to improve the objective functions.

In summary, in this algorithm, N_p trial individuals are generated using these steps and each trial individual is evaluated for its values of objective functions and constraints. These trial individuals are mixed with the current population, and non-dominated sorting of the combination population followed by crowding distance calculations are performed to select the individuals for next generations able to improve the objective functions. In this multi-objective method, the inequality constraints are handled by the feasibility approach (constraint dominance) of Deb et al. [30].

This multi-objective optimization procedure is followed by a complementary analysis on representative spots from each Pareto front in order to obtain general trends on controllability, thermodynamic efficiency and CO_2 emissions for each sequence.

The multi-objective optimization and complementary studies have been performed for the different alternative sequences (using cryogenic extractive distillation) and different pure entrainers. Besides those, the conventional chemical absorption method is presented for comparison purposes.

The nature of the independent decision variables manipulated for each sequence observed several heuristic rules, representing the system on the mass balances (flow distribution), the energy requirements (reflux ratio, among others) and the design parameters (number of trays, etc.)

Thus, mixed-integer variables were selected like stages, reflux ratios, product flows, among others. Moreover, the separation processes must satisfy restrictions of performance related to the

product purities. Details of the restrictions used for every case are described in Section 7.

5. Methodology for the performance evaluation of the separation processes

The Aspen Plus 7.0 simulator, Excel 2007 and Visual Basic 6.3 were utilized for the multi-objective optimization method [29].

5.1. Multi-objective optimization of the design alternatives

Due to the fact that the optimizer requires some initial guesses and suitable ranges of variation for the decision variables along the optimization, a preliminary sensitivity analysis was performed for all the cases studied. Moreover, different solvents were considered to select the best entrainer for the alternative design sequences.

In order to ensure a truthful preliminary sensitivity analysis, different standards were fixed:

1. The purity of the product streams: 0.9 for the CO_2 and ethane and 0.93 for the solvent streams, both on molar basis.
2. The percentage of the carbon dioxide removal for the schemes: 96, 97, 98, 98.5, 99, 99.5 and 99.9%, on molar basis.

Due to the presence of the ethane–carbon dioxide azeotrope that makes the separation process challenging, these values of purity and removal were arbitrary fixed in order to find different initial scenarios of performance (energy consumption, capital cost, and value of decision variables) for all the sequences studied.

In the case of the thermally coupled distillation sequence, the starting procedure was supplemented by the methodology proposed by Hernández and Jiménez [9]. The general procedure for the starting simulations is described in Fig. 5.

After this stage, the best two sequences per each case were selected for the multi-objective optimization. At this point, just the purity restrictions were kept in order to get the configurations with higher purities. The multi-objective DE requires the following parameters: population size (N_p), crossover probability (Cr) and mutation factor (F). The objective functions were the minimization of the total annual cost (TAC) and the maximization of the carbon dioxide removal. The TAC function is shown in Eq. (2).

$$TAC = \sum \left[\left(\frac{\text{capital cost}}{\text{time of investment}} \right)_i + (\text{cost of utilities})_i \right] \quad (2)$$

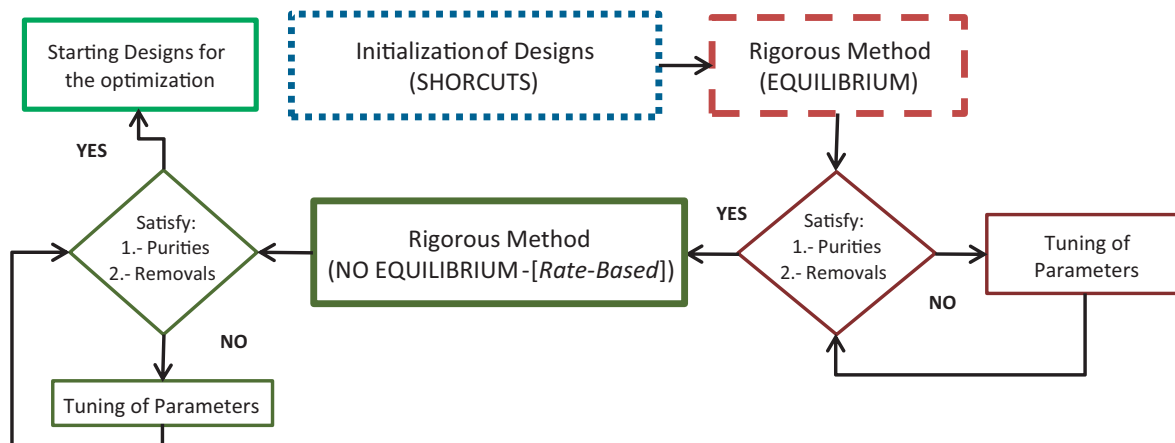


Fig. 5. General procedure for starting designs.

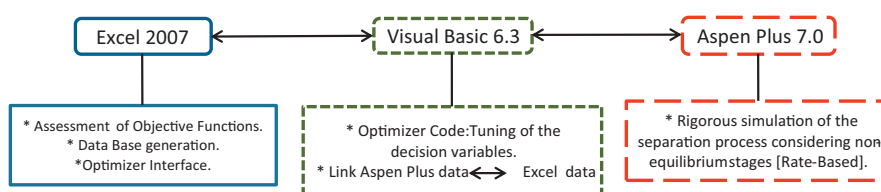


Fig. 6. Flowchart of the hybrid platform for the optimization procedure.

As regards for the optimization procedure, the simulations with lower purities than those established by the boundaries set above were penalized. Thus, schemes with equal or greater purities were favored.

Regarding the capital cost evaluation on TAC, the correlations and data were taken from Turton et al. [31]. Distillation columns, condensers, reboiler, vessels, compressors and pumps were taken into account. For this objective function, 10 years of investment and 8500 h of service per year were fixed in all the cases.

The energy costs associated to steam, cooling water, refrigerant, electricity were evaluated according to Turton et al. [31].

The multi-objective optimization was made using the hybrid platform depicted in Fig. 6. During the evolution of the algorithm, the vector values of decision variables (V_x) are transferred from Microsoft Excel to Aspen Plus using DDE (dynamic data exchange) by COM technology. These values are attributed in Excel to the corresponding process variables (V_p) and then sent to Aspen Plus. Note that using the COM technology; it is possible to add a code so that the applications behave as an Object Linking and Embedding (OLE) automation server. After running the rigorous simulation, Aspen Plus returns to Microsoft Excel the vector of results (V_r). Finally, Excel analyzes the objective function (F_{OB}) value for the optimization procedure.

5.2. Complementary analysis

After the optimization, Pareto fronts (%CO₂ removed versus TAC) were obtained, and 10 operating conditions obtained from each Pareto front were chosen. These points were suitable distributed, thus they represent properly the general tendency of the Paretos, and then it was carried out three different studies in a similar hybrid platform:

(a) *Controllability analysis by singular value decomposition (SVD)*: for this study, it was used the concept of dominant time constant with a linear first-order response for the columns, defined by Skogestad and Morari [32], to generate the transfer matrix of the process. This assumption let to generate the dominant time

constant from steady-state simulations, considering that the distillation columns dynamics are dominated by one large time constant. Next, by means of the frequency response, it was accomplished the SVD, Eq. (3), with a constant disturbance (+0.3%) on the control variable directly related to the product stream, [33].

The SVD theorem defines a matrix $A \in R_r^{m \times n}[C_r^{m \times n}]$, and the existence of orthogonal-unitary matrixes $U \in R_r^{m \times m}[C_r^{m \times m}]$ and $C \in R_r^{n \times n}[C_r^{n \times n}]$ that defines the SVD as Eq. (3) describes.

$$A \in U \Sigma V^T [U \Sigma^H] \quad (3)$$

where $\Sigma = \text{diag}(\sigma^*, \dots, \sigma_*)$ with $\sigma^* \geq \dots \geq \sigma_* > 0$, R is the real domain C the complex domain A^T the transpose of A and A^H the conjugated transpose of A . The control properties derived from the SVD analysis are the condition numbers and minimum singular values. The first quantifies the sensitivity of the system with respect to errors on modeling, non-linearity and disturbances; meanwhile, the second reflects potential problems of the system under feedback control.

The product streams' purity is one of the most common variables analyzed for initial controls studies on distillation columns [34–36]; then, the only output variable studied for each product stream was the molar fraction. For instance, if the molar fraction of component i in the distillate flow was defined as output variable, the selected control variable directly related to the distillate purity is the reflux ratio. In the same way, for the molar fraction of component j in the bottom flow, the selected control variable directly related to the residue purity is the reboiler duty. Finally, regarding the molar fraction of the component k in the side stream, the flow rate was selected as control variable directly related to its purity.

Table 6 summarizes the input and output variables and disturbances as well for all the case studies.

A typical transfer matrix of the process, suitable for the SVD analysis, is here reported:

$$\begin{bmatrix} x_{\text{CO}_2} \\ x_{\text{Ethane}} \\ x_{\text{Entrainer}} \end{bmatrix} = \begin{bmatrix} g_{1,1}(\omega, \tau_{c1}) & g_{1,2}(\omega, \tau_{c2}) & g_{1,3}(\omega, \tau_{c3}) \\ g_{2,1}(\omega, \tau_{c1}) & g_{2,2}(\omega, \tau_{c2}) & g_{2,3}(\omega, \tau_{c3}) \\ g_{3,1}(\omega, \tau_{c1}) & g_{3,2}(\omega, \tau_{c2}) & g_{3,3}(\omega, \tau_{c3}) \end{bmatrix} \begin{bmatrix} RR_1 \\ RR_2 \\ Q_2 \end{bmatrix} \quad (4)$$

where x represents the molar fraction, g the transfer function, τ_{ci} the dominant time constant for each disturbance realized, ω the frequency space, RR the reflux ratio and finally Q represents the reboiler heat duty. The subscripts 1 and 2 refer to the number of the distillation column.

(b) *Thermodynamic efficiency*: this study is based on the methodology described by Seader and Henley [37]. The analysis, reported from Eq. (5)–(8), was carried out for the whole processes defined in the cases of study, including also the refrigeration cycles.

$$\sum_{\text{Out}} \left[n_i b_i + Q_j \left(1 + \frac{T_0}{T_{s,j}} \right) + W_{s,k} \right] - \sum_{\text{in}} \left[n_l b_l + Q_m \left(1 + \frac{T_0}{T_{s,m}} \right) + W_{s,n} \right] = LW \quad (5)$$

$$b = (h - T_0 S) \quad (6)$$

$$\eta = \frac{W_{\min}}{LW + W_{\min}} \quad (7)$$

$$LW = T_0 \cdot \Delta S_{\text{irr}} \quad (8)$$

where n represents the number of moles, b is the minimum work of separation [kJ/mol], Q is the heat flow [kJ/mol], T_0 is the temperature of the surroundings [K], T_s is the temperature of the reservoir [K], W_s is the shaft work [kJ/h], h is the specific enthalpy [kJ/mol], S is the specific entropy [kJ/molK], LW is the loss of work in the system [kJ/h], ΔS_{irr} is the entropy increasing due to irreversibility [kJ/molK] and finally η is the thermodynamic efficiency.

All the thermodynamic properties, like enthalpies and entropies of the streams, were evaluated through the use of the process simulator Aspen Plus V7.0 for all the input and output streams.

(c) *CO₂ emissions*: this analysis was performed based on the work of Gadalla et al. [38] and reported in Eqs. (9) and (10). The CO₂ emissions were considered as generated by the steam used in the reboiler of the columns when methane is used as a fuel.

$$Q_{\text{fuel}} = \left(\frac{Q_{\text{proc}}}{\lambda_{\text{proc}}} \right) (h_{\text{proc}} - 419) \left(\frac{T_{\text{FTB}} - T_0}{T_{\text{FTB}} - T_{\text{stack}}} \right) \quad (9)$$

$$\text{CO}_{2\text{Emiss}} = \left(\frac{Q_{\text{fuel}}}{\text{NHV}} \right) \left(\frac{C\%}{100} \right) \left(\frac{3600}{1000} \right) \alpha \quad (10)$$

where Q_{proc} is the reboiler duty [kJ/h], λ_{proc} [kJ/kg] and h_{proc} [kJ/kg] are the latent heat and enthalpy of steam delivered to the process respectively, while T_{FTB} [°C] is the flame temperature of the boiler flue gases and T_{stack} [°C] and T_0 are the temperature stack and of the surroundings, respectively. NVH is the net heat value of fuel [kJ/kg], α is the molar ratio of CO₂ and C, C% is the carbon amount in fuel, Q_{fuel} the heat generated by the fuel in the reboiler [kJ/h] and $\text{CO}_{2\text{Emiss}}$ the CO₂ emissions [kg/h].

After the Pareto fronts and the post-optimization analyses were obtained, a comparison between sequences was accomplished.

6. Case studies

The sour feed composition was defined only considering the CO₂ and the ethane in the proportion inside the boundaries proposed by the Natural Gas Supply Association [39]. Then, it was assumed ethane as the only relevant hydrocarbon in the natural gas because the present study is mainly focused on the carbon dioxide–ethane azeotropic separation and it is also reasonable consider that the methane has been already removed in another unit operation. Moreover after the methane, the ethane is the second major component.

The feed composition on molar basis, the temperature and the pressure analyzed are: 67.78% ethane and 32.22% CO₂, 67 °C and 75.84 bar, respectively.

The pressure and temperature of operation, and the starting values of the entrainer flows for the alternative sequences were taken from the work of Lastari et al. [40]. All the conditions for the chemical absorption process were taken from POGC [41]. For all the schemes, the rate based model and sieve trays columns were utilized.

The conventional cryogenic extractive distillation (Fig. 2), the cryogenic extractive distillation sequence with side rectifier (Fig. 3) and the alternative Petlyuk sequence (Fig. 4) were simulated considering four different pure solvents: propane, n-butane, n-pentane and n-hexane. As benchmark process, the configuration with chemical absorption by an aqueous solution of methanol-amine (MEA) (6.86% MEA and 93.14% water on molar basis) reported in Fig. 1, was analyzed as well.

Regarding the optimization, the starting values for the multi-objective DE method were established based on preliminary calculations and the selected values were: $N_p = 10$ *number of decision variables, $F = 0.8$ and $Cr = 0.9$. The stopping criterion of the multi-objective method, based on the number of generations, was fixed equal to 160 for all the optimizations performed. This choice was based on the clearness of Pareto fronts obtained for the CCED and CEDSR sequences considered like tuning procedure.

7. Analysis of results

In this section, the results will be presented according to the same order used for the Methodology already described.

7.1. Multi-objective optimization for the design of separation processes

According to Fig. 7, among all the solvents n-butane and n-pentane were the most promising ones. In general the n-butane has the lowest TAC in most of the schemes defined. Comparing all the sequences, it is possible to notice that the conventional scheme (CCED) and the thermally coupled sequence (CEDSR) have the lower TAC values. After the initial design was obtained, it was defined the optimization problem for each sequence studied.

These optimization problems are given below.

7.1.1. Conventional cryogenic extractive distillation (CCED)

$$\min(\text{TAC}), \max(\text{FCO}_2) = f(S1, RR1, FS1, ES, EF, D1, DF1, S2, FS2, D2, RR2, DF2)$$

Subject to

$$y_m \geq x_m$$

$$\text{Limit}_{\text{lower},i} \leq x_{\text{var},i} \leq \text{Limit}_{\text{upper},i}$$

where $i = 1, 2, 3, \dots, n$ number of decision variables.

Where TAC is the total annual cost, FCO_2 represents the CO₂ flow rate, S, D, RR and DF are the number of stages, diameter, reflux ratio and flow of distillate in each of the two columns. The FS represents the feed stage for each equipment. ES is the entrainer stage and EF the entrainer flow in the extractive distillation column. All the flows are in kmol/hr and the diameter in meters. Finally y_m is a vector that represents the product purities obtained through simulation of the processes for the m components; meanwhile the x_m represents the restrictions defined for the respective product purities for the m components. $\text{Limit}_{\text{lower}}$ and $\text{Limit}_{\text{upper}}$ represent the lower and

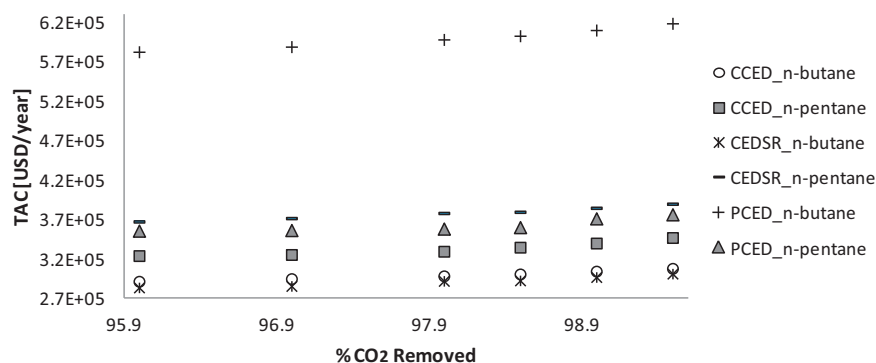


Fig. 7. The best alternative processes for the sensitivity analysis. % of removal on molar basis.

upper constraints for the decision variable x_{var} for each i variable manipulated. A total of 12 variables were manipulated.

7.1.2. Cryogenic extractive distillation with side rectifier (CEDSR)

$$\min(\text{TAC}), \max(\text{FCO}_2) = f(S1, \text{RR}, \text{FS}, \text{ES}, \text{EF}, \text{D1}, \text{DF1}, \text{S2}, \text{VF}, \text{D2}, \text{LFS}, \text{DF2})$$

Subject to

$$y_m \geq x_m$$

$$\text{Limit}_{\text{lower},i} \leq x_{var,i} \leq \text{Limit}_{\text{upper},i}$$

where $i = 1, 2, 3, \dots, n$ number of decision variables.

Where TAC is the total annual cost, FCO_2 is the CO_2 flow rate, S, D and DF are the number of stages, diameter and flow of distillate in each of the two columns. The FS and RR represent the feed stage and reflux ratio of the first column. ES is the entrainer stage and EF the entrainer flow in the extractive distillation column. The VF and LFS are the vapour flow and the liquid flow stage of interconnection between the main column and the side rectifier. All the flows are in kmol/h and the diameter in meters. Finally, y_m is a vector that represents the product purities obtained through simulation of the processes for the m components; meanwhile the x_m represents the restrictions defined for the respective product purities of the m components. $\text{Limit}_{\text{lower}}$ and $\text{Limit}_{\text{upper}}$ represent the lower and upper constraints for the decision variable x_{var} for each i variable manipulated. A total of 12 variables were manipulated.

7.1.3. Petlyuk cryogenic extractive distillation (PCED)

$$\min(\text{TAC}), \max(\text{FCO}_2) = f(S, \text{RR}, \text{FS}, \text{ES}, \text{EF}, \text{D1}, \text{DF}, \text{LF}\alpha, \text{LFS}\alpha, \text{D2}, \text{VFb}, \text{VFSb}, \text{SSF}, \text{SSS})$$

Subject to

$$y_m \geq x_m$$

$$\text{Limit}_{\text{lower},i} \leq x_{var,i} \leq \text{Limit}_{\text{upper},i}$$

where $i = 1, 2, 3, \dots, n$ number of decision variables.

Where TAC is the total annual cost, FCO_2 is the CO_2 flow rate, D is the diameter in each of the two columns. The FS, RR, S and DF represent the feed stage, reflux ratio and distillate flow of the first column. ES is the entrainer stage and EF the entrainer flow in the extractive distillation column. According to Fig. 4, LFa and LFSa

are the flow and the stage of the liquid flow of the interconnection stream between the main column and the post-fractionator. In a similar way, the VFb and VFSb are the flow and the stage of the vapour flow of the interconnection stream between the main column and the post-fractionator. The number of stages in the post-fractionator was defined according to the position of the LFa and VFb streams since they represent the upper limit and the lower limit of the post-fractionator respectively. The variables SSF and SSS are the flow rate and the stage tray of the side stream of the post-fractionator. All the flows are in kmol/hr and the diameter in meters. Finally y_m is a vector that represents the product purities obtained through simulation of the processes of the m components; meanwhile the x_m represents the restrictions defined for the respective product purities of the m components. $\text{Limit}_{\text{lower}}$ and $\text{Limit}_{\text{upper}}$ represent the lower and upper constraints for the decision variable x_{var} for each i variable manipulated. A total of 14 variables were manipulated.

7.1.4. Conventional chemical absorption system (CCAS)

$$\min(\text{TAC}), \max(\text{FCO}_2) = f(S1, \text{SF}, \text{D1}, \text{S2}, \text{FS}, \text{D2}, \text{RR}, \text{FD})$$

Subject to

$$y_m \geq x_m$$

$$\text{Limit}_{\text{lower},i} \leq x_{var,i} \leq \text{Limit}_{\text{upper},i}$$

where $i = 1, 2, 3, \dots, n$ number of decision variables.

Where TAC is the total annual cost, FCO_2 is the CO_2 flow rate, S and D are the number of stages and diameter in each column. The SF is the solvent flow for the absorber. FS, RR and FD represent the feed stage, reflux ratio and the flow of distillate of the second column. All the flows are in kmol/hr and the diameter in meters. Finally y_m is a vector that represents the product purities obtained through simulation of the processes for the m components; meanwhile the x_m represents the restrictions defined for the respective product purities of the m components. $\text{Limit}_{\text{lower}}$ and $\text{Limit}_{\text{upper}}$ represent the lower and upper constraints for the decision variable x_{var} for each i variable manipulated. A total of 8 variables were manipulated.

7.2. Summary of multi-objective results

The data here presented satisfied all the constraints defined above, except for the case of the PCED sequence where the purity constraints were not respected.

As reported in Fig. 8, the CEDSR configuration with n-butane as entrainer reached the lowest TAC.

In the optimization, the product streams' purity of CO_2 , ethane and solvents obtained were greater than those used for the preliminary sensitivity analysis, mainly in the entrainer stream. As consequence, most of the values on the manipulated variables were

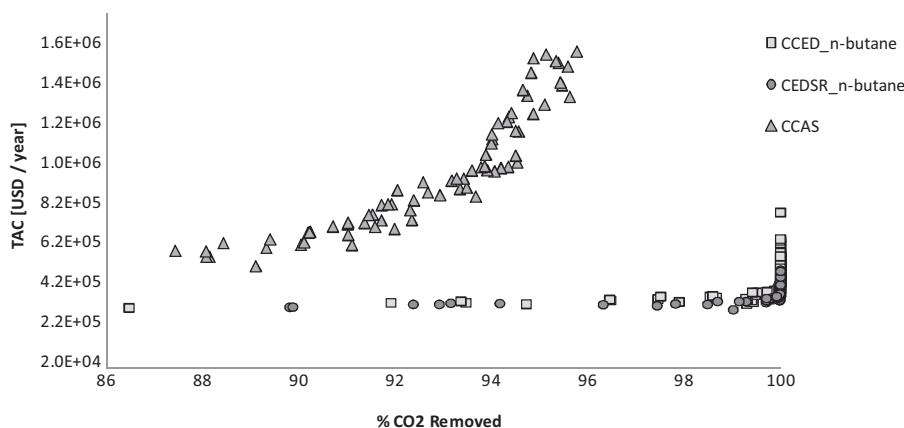


Fig. 8. The best sequences after optimization. % of removal on molar basis.

higher as well. The interconnecting flows between columns were the decision variables with more fluctuations.

All the alternative arrangements reached out a very high removal of the acid gas (up to 100%) included PCED; nevertheless, PCED Pareto fronts were not so clear. For the case of the CCAS, less carbon dioxide removals were obtained and the costs were higher compare to all the alternatives.

In order to show the lower and upper constraints of decision variables, and also the main results of the design of the sequences above described, one individual of each Pareto front (the point just before the exponential increase on TAC) was selected and the results summarized in Tables 1–4.

Note that for CCAS the solvent is a binary mixture, then the restriction for the solvent stream was defined as the fraction of MEA recycled by the system (molar basis), as reported in Table 4.

For PCED case, it seems that the decision variables related to the total number of stages and the side stream flow are close to the upper limits; thus, the PCED designs with bigger columns and less product rate of CO₂ and/or entrainer recycled might meet the purity restrictions of the product streams.

Analysing in general terms the decision variables for the optimized sequences, we can detect several patterns depending on

which perspective is considered. If we focused on the solvents, the use of n-butane is associated to configurations with higher amount of solvent and number of stages, but a lower reflux ratio than the schemes using n-pentane like entrainer is required.

On the other hand if we focused on the type of sequence, CEDSR needs less amount of solvent and reflux ratios than CCED and PCED. This difference is not so relevant between CCED and CEDSR, but significance with respect to PCED.

High amount of entrainer and reflux ratios influence negatively the total annual cost on the CCAS scheme.

Finally, according to Fig. 8, CEDSR using the n-butane is the sequence with lowest TAC. We can analyze the changes of some of their decision variables for different CO₂ removals. Fig. 9 shows 4 of the 12 decision variables manipulated during the optimization.

If we want to increase the CO₂ removal for the scheme CEDSR, we need to increase the amount of fresh entrainer, the number of stages of the total sequence, the reflux ratio (RR) of column I (C I), and lastly the amount of the interconnecting flow LF. These results reflect foreseen patterns: higher removals require more energy (for CEDSR, RR C I ≫ RR C II) and/or bigger equipments. Regarding the make-up of the entrainer, the increase of this amount was foreseen

Table 1
Restrictions on the decision variables and main results of a representative sequence CCED n-butane and n-pentane. Note that the definition, and therefore the numerical values of α , β and γ are depicted in the column “Variables and results” of the same table. The symbol * implies a product that is only rounded on integer variables.

Variables and results	n-Butane		n-Pentane		Representative sequence selected	
	Limit _{lower}	Limit _{upper}	Limit _{lower}	Limit _{upper}	n-Butane	n-Pentane
Number of stages C I (α)	60	100	50	100	95	63
Feed stage C I (β)	0.15*(α)	0.7*(α)	0.2*(α)	0.7*(α)	52	31
Entrainer stage	0.01*(β)	0.4*(β)	0.01*(β)	0.4*(β)	10	2
Entrainer make-up (kmol/h)	1.50	7.50	1.50	6.50	4.69	3.32
Diameter C I (m)	0.40	1.00	0.50	1.10	0.72	0.73
Reflux ratio C I	3.00	10.00	4.00	13.00	6.42	7.80
Number of stages C II (γ)	5	50	5	50	29	24
Feed stage C II	0.1*(γ)	0.5*(γ)	0.1*(γ)	0.6*(γ)	7	13
Diameter C II (m)	0.50	1.10	0.50	1.10	0.78	0.90
Reflux ratio C II	0.01	5.00	0.01	6.00	0.45	0.24
Distillate flow C I (kmol/h)	12.22	15.22	12.22	15.22	14.53	14.48
Distillate flow C II (kmol/h)	26.81	29.81	26.81	29.81	29.45	27.93
Purity of CO ₂ stream	0.9	1	0.9	1	0.9096	0.9122
Purity of ethane stream	0.9	1	0.9	1	0.9004	0.9550
Purity of entrainer/solvent stream	0.93	1	0.93	1	1.0000	0.9909
Condenser duty C I (kW)	–	–	–	–	–341.05	–419.60
Reboiler duty C I (kW)	–	–	–	–	209.08	210.58
Condenser duty C II (kW)	–	–	–	–	–135.67	–111.22
Reboiler duty C II (kW)	–	–	–	–	192.87	246.04
Pressure C I and II (bar)	–	–	–	–	24.15	24.15
Total cost (USD/year)	–	–	–	–	4.03E+05	4.61E+05

Table 2

Restrictions on the decision variables and main results of a representative sequence CEDSR n-butane and n-pentane. Note that the definition, and therefore the numerical values of α and β are depicted in the column “Variables and results” of the same table. The symbol * implies a product that is only rounded on integer variables.

Variables and results	n-Butane		n-Pentane		Representative sequence selected	
	Limit _{lower}	Limit _{upper}	Limit _{lower}	Limit _{upper}	n-Butane	n-Pentane
Number of stages C I (α)	60	110	60	110	99	85
Feed stage (β)	0.1*(α)	0.6*(α)	0.1*(α)	0.5*(α)	40	38
Entrainer stage	0.01*(β)	0.4*(β)	0.01*(β)	0.35*(β)	4	2
Entrainer make-up (kmol/h)	2.00	8.00	2.00	7.50	4.49	3.05
Diameter C I (m)	0.45	1.10	0.65	1.20	0.79	0.94
Reflux ratio C I	5.00	12.00	5.00	13.00	5.97	8.65
Number of stages C II	5	55	5	55	37	8
Liquid flow stage	0.6*(α)	0.95*(α)	0.65*(α)	0.95*(α)	85	79
Diameter C II (m)	0.61	0.93	0.61	0.93	0.61	0.93
Vapor flow (kmol/h)	15.00	50.00	20.00	60.00	30.39	37.61
Distillate flow C I (kmol/h)	12.22	15.22	12.22	15.22	14.56	14.62
Distillate flow C I (kmol/h)	26.81	29.81	26.81	29.81	29.14	27.02
Purity of CO ₂ stream	0.9	1	0.9	1	0.9082	0.9041
Purity of ethane stream	0.9	1	0.9	1	0.9155	0.9815
Purity of entrainer/solvent stream	0.93	1	0.93	1	0.9989	0.9793
Condenser duty C I (kW)	–	–	–	–	–325.19	–464.97
Reboiler duty C I (kW)	–	–	–	–	348.13	552.41
Condenser duty C II (kW)	–	–	–	–	–97.63	–156.48
Pressure C I and II (bar)	–	–	–	–	24.15	24.15
Compressor C III (kW)	–	–	–	–	1.36	1.03
Total cost (USD/year)	–	–	–	–	3.69E+05	5.64E+05

as well; nevertheless we expected a more variable behavior in the LF values. The augment on the solvent make-up was reflected in bigger internal flows between columns in order to set-off the mass balances. The most relevant information about Fig. 9 is to identify the intervals of values (rectangles) for the decision variables that allow high CO₂ removals at still low TAC.

Regarding the amplitude ranges of the decision variables constraints; there was not an important difference between solvents and among extractive sequences as well. On the other hand, the amplitude ranges for the scheme CCAS was narrower than

others because of the higher restrictions on the model for ensuring convergence.

In general terms, we noted that the cost utilities were the dominant factor on the TAC, representing around the 90–95% of the total value.

Besides, if we observed the Pareto fronts obtained during the optimization, we can detect certain fluctuations of the values on the trends. The random elements of the optimizer strategy and the not properly parametric tuning of the optimizer may have made these fluctuations.

Table 3

Restrictions on the decision variables and main results of a representative sequence PCED n-butane and n-pentane. Note that the definition, and therefore the numerical values of α , β , γ and δ are depicted in the column “Variables and results” of the same table. The symbol * implies a product that is only rounded on integer variables.

Variables and results	n-Butane		n-Pentane		Representative sequence selected	
	Limit _{lower}	Limit _{upper}	Limit _{lower}	Limit _{upper}	n-Butane	n-Pentane
Number of stages C I (α)	75	125	75	120	122	112
Feed stage C I (β)	0.4*(α)	0.75*(α)	0.4*(α)	0.7*(α)	71	64
Entrainer stage	0.01*(β)	0.35*(β)	0.01*(β)	0.35*(β)	4	3
Entrainer make-up (kmol/h)	2.00	12.00	2.00	11.00	6.60	6.00
Diameter C I (m)	0.75	1.35	0.60	1.25	1.00	0.91
Reflux ratio C I	5.00	20.00	7.00	20.00	10.00	10.63
LFa stage (γ)	0.5*(σ)	0.85*(σ)	0.5*(σ)	0.85*(σ)	101	91
LFa (kmol/h)	22.00	60.00	30.00	65.00	38.75	46.57
VFb stage (δ)	{(α) – (γ)}*0.15 + (γ)	{(α) – (γ)}*0.85 + (γ)	{(α) – (γ)}*0.2 + (γ)	{(α) – (γ)}*0.85 + (γ)	107	99
VFb (kmol/h)	10.00	60.00	20.00	70.00	13.92	50.31
Distillate flow C I (kmol/h)	13.00	16.22	12.22	16.22	15.50	15.00
Diameter C II (m)	0.35	0.98	0.35	0.98	0.63	0.73
SSF stage	{(δ) – (γ)}*0.4	{(δ) – (γ)}*0.9	{(δ) – (γ)}*0.35	{(δ) – (γ)}*0.9	4	7
SSF (kmol/h)	26.50	30.81	26.81	30.81	30.00	30.19
Purity of CO ₂ stream	0.9	1	0.9	1	0.8528	0.8816
Purity of ethane stream	0.9	1	0.9	1	0.8519	0.8616
Purity of entrainer/solvent stream	0.93	1	0.93	1	0.9454	0.9557
Condenser duty C I (kW)	–	–	–	–	–527.47	–550.66
Reboiler duty C I (kW)	–	–	–	–	445.14	447.77
Pressure C I and II (bar)	–	–	–	–	24.15	24.15
Compressor C III (kW)	–	–	–	–	0.79	2.86
Compressor C IV (kW)	–	–	–	–	0.55	2
Total cost (USD/year)	–	–	–	–	4.53E+05	4.71E+05

Table 4
Restrictions on the decision variables and main results of a representative sequence CCAS. Note that the definition, and therefore the numerical values of α is depicted in the column “Variables and results” of the same table. The symbol * implies a product that is only rounded on integer variables.

Variables and results	Limit _{lower}	Limit _{upper}	Representative sequence selected
Number of stages C I	10	30	19
Solvent make-up (kmol/h)	235.00	252	249.63
Diameter C I (m)	0.65	1.35	0.83
Number of stages C II (α)	20	70	59
Feed stage C II	0.15* (α)	0.7* (α)	35
Reflux ratio C II	5.00	15	10.15
Diameter C II (m)	0.80	1.5	1.20
Distillate flow C II(kmol/h)	11.20	13.7	12.25
Purity of CO ₂ stream	0.9	1	0.9124
Purity of ethane stream	0.9	1	0.9873
* Fraction of MEA's flow recycled	0.93	1	0.9999
Condenser duty C II (kW)	-	-	-1548.15
Reboiler duty C II (kW)	-	-	1778.89
Pressure C I (bar)	-	-	24.15
Pressure C II (bar)	-	-	1.82
Cooler C III (kW)	-	-	-141.70
Pump_C IV (kW)	-	-	9.82
Pump_C V (kW)	-	-	9.05
Total cost (USD/year)	-	-	1.03E+06

7.3. Complementary analysis

The comparisons of the results presented in this section are based on the CEDSR sequence selected as the best option during the optimization step.

As reported in Fig. 10(a), the thermodynamic efficiency (η) has a nonlinear decreasing trend due to the fact that at high gas acid removal the efficiency is lower because of the increment in the system energy demand. However, the relation between energy consumption and thermodynamic efficiency is not as simple and direct as the energy consumption and the amount of CO₂ generated in the reboiler, see Fig. 10(b). The CEDSR sequence presented a lower efficiency that the CCAS system because of the use of refrigerants in the extractive distillation process and for the higher CO₂ removals.

Concerning the CO₂ emissions (CO₂ generated), the tendencies were the same of the TAC reported in the first Pareto fronts, see Fig. 8. The CEDSR sequence generates less CO₂ in its reboiler than the total CO₂ removed by the scheme. In the case of the CCAS sequence, this panorama was less favorable as shown in Fig. 10(b).

Finally in this dynamic study, the condition number quantifies the sensitivity of the system with respect to errors on modeling, non-linearity and disturbances; thus, smaller condition numbers are preferred. High values of the reciprocal of the minimum singular value makes evident potential problems of the system

Table 5
Description of the points depicted in Figs. 11 and 12, sequence CEDSR n-butane and CCED n-butane; molar basis.

Point	CEDSR n-butane		CCED n-butane	
	kUSD/year	% CO ₂ Removed	kUSD/year	% CO ₂ Removed
1.00	344.47	98.48	384.41	98.54
2.00	317.68	99.02	379.53	98.67
3.00	357.39	99.30	346.81	99.30
4.00	353.78	99.70	391.69	99.48
5.00	375.49	99.83	398.34	99.84

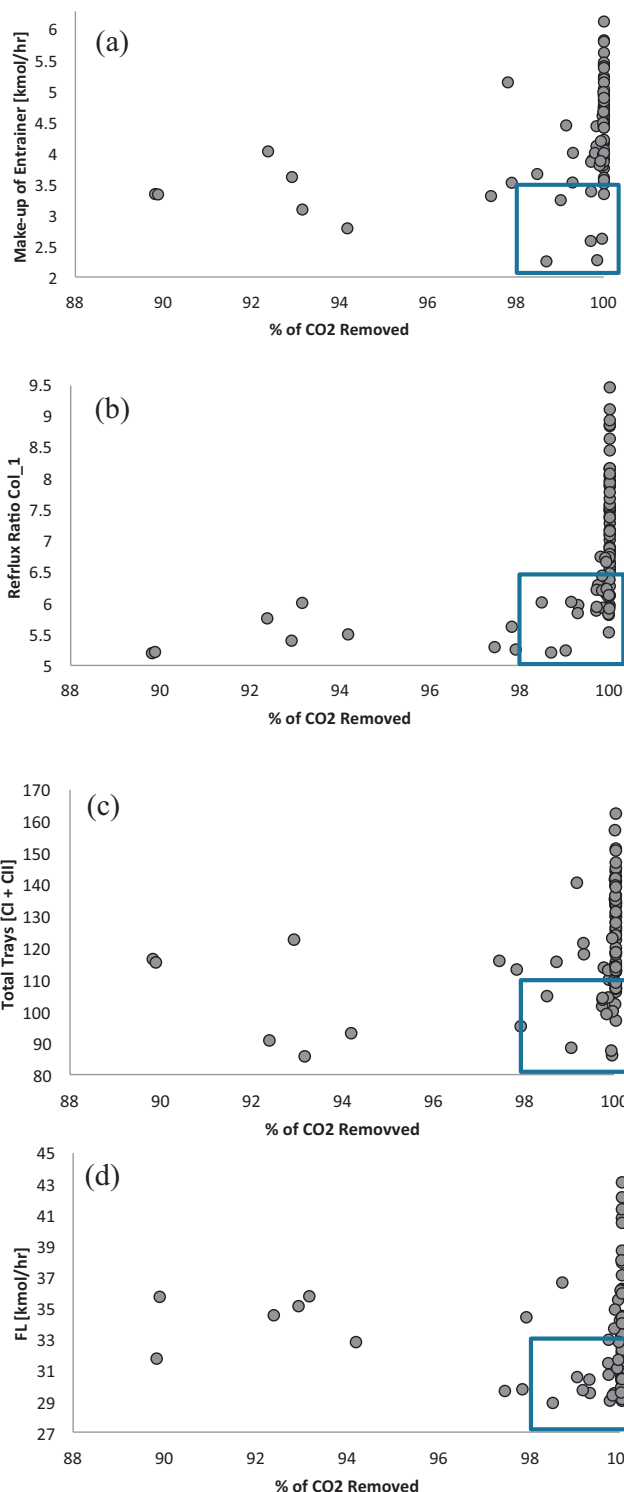


Fig. 9. (a) Make-up of entrainer, (b) reflux ratio C I, (c) total trays (C I and C II), (d) FL flow. All these variables at different CO₂ removals for the sequence CEDSR using n-butane. % of removal on molar basis.

under feedback control, then higher minimum singular values are sought.

Fig. 11(a) and (b) show the condition numbers and singular values of operating conditions with high carbon dioxide removal and reasonable TAC for CEDSR (just before the exponential increasing on TAC, 98 to 99.9% of CO₂ removed), see Table 5, are depicted. This region, named “region of analysis”, is characterized by a suitable

Table 6
General information for controllability analysis.

Sequence	Control inputs			Control outputs	Disturbances on the control inputs
CCED	Reflux ratio C I	Reflux ratio C II	Reboiler duty C II	Molar fraction of CO ₂ , ethane and entrainer on the product stream directly related to each control input	+0.3%
CEDSR	Reflux ratio C I	Reflux ratio C II	Reboiler duty C II	Molar fraction of CO ₂ , ethane and entrainer on the product stream directly related to each control input	+0.3%
PCED	Reflux ratio C I	Reboiler duty C I	Flow rate C II	Molar fraction of CO ₂ , ethane and entrainer on the product stream directly related to each control input	+0.3%
CCAS	Reflux ratio C I	Reboiler duty C I		Molar fraction of CO ₂ and ethane on the product stream directly related to each control input	+0.3%

performance (low TACs and high CO₂ removals) and dynamic properties (low condition numbers and high minimum singular values). The extreme points (far from the region of analysis) in the Pareto fronts showed the worst dynamic features, especially those that had the highest removal of acid gas and thus, the higher TAC. For the CCAS scheme, the worst dynamic properties were estimated for the intermediate region into the Pareto front.

Moreover, as purposes of comparison, Fig. 12 and Table 5 represent the spots for the same region of analysis of the CCED sequence using n-butane as entrainer. We can see that their dynamic attributes are comparable.

The matrixes of transfer functions for each design described in Tables 1–4 are shown in Tables 7–13.

If we compare these matrixes, general trends are found. For instance, the gain and dominant-constant time for the first manipulated variable were the biggest. For all the sequences this variable was the reflux ratio of the first column (except CCAS, where the solvent recovery column was the one studied under this dynamic analysis). The magnitudes of gains and dominant-constant times for the other two variables were of the same order.

Doing the comparison between schemes, the magnitude of the gains were too similar; nevertheless, the dominant-constant time not. The CCAS had the lowest values, followed by the CEDSR, CCED and lastly the PCED. This time represents indirectly the controllability; higher dominant-constant time reflects, partially, poorer dynamic properties. Inside the extractive sequences, CEDSR presented the most proper dominant-constant times, meanwhile PCED presented the worst. Difference between times on CEDSR and CCED was minor. Finally if we compare the effect of the solvents, the n-butane increased the gain and dominant-constant time of the first variable manipulated, whereas n-pentane increased them on the second and third variables. In general terms, both solvent's effects were compensated in certain form.

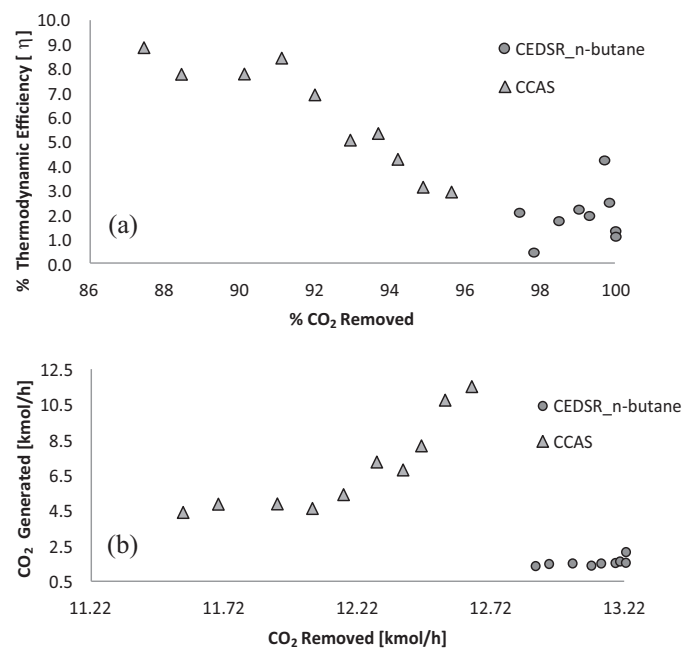


Fig. 10. (a) Thermodynamic efficiency, (b) CO₂ emissions for the best alternative sequence and for the conventional chemical absorption. % of removal on molar basis.

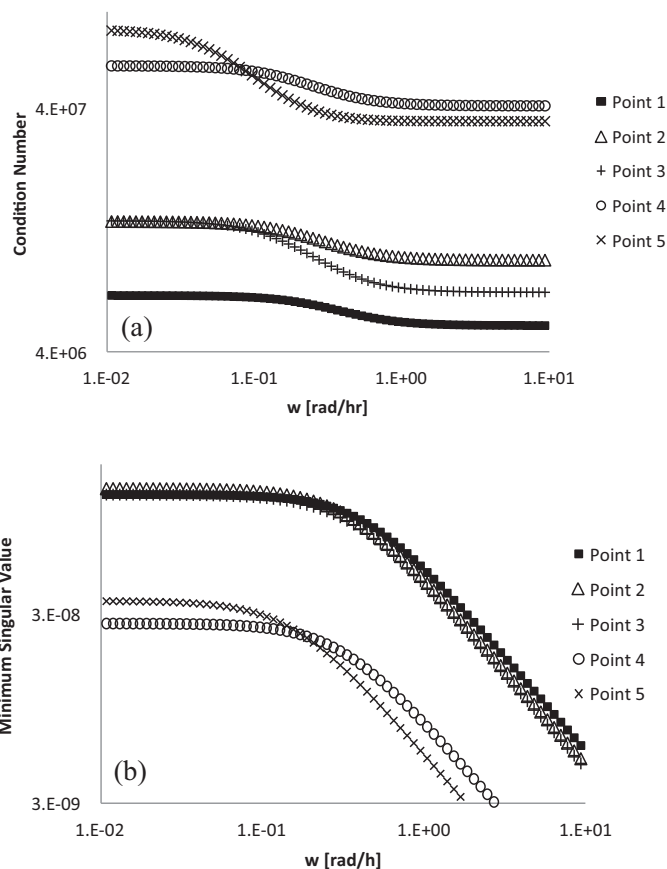


Fig. 11. (a) Condition Number, (b) minimum singular values for representative spots inside the “region of analysis” of the sequence CEDSR n-butane.

Table 7
Matrix transfer function for the CCED sequence, using n-butane as entrainer.

$$\begin{bmatrix} \frac{2.663 - 51.873\omega j}{1 + 379.404\omega^2} & \frac{1.23 \times 10^{-4} - 1.84 \times 10^{-4}\omega j}{1 + 2.245\omega^2} & \frac{-2.85 \times 10^{-7} + 5.20 \times 10^{-7}\omega j}{1 + 3.332\omega^2} \\ \frac{-2.674 + 52.080\omega j}{1 + 379.404\omega^2} & \frac{0.181 - 0.271\omega j}{1 + 2.245\omega^2} & \frac{-0.999 + 1.823\omega j}{1 + 3.332\omega^2} \\ \frac{0.011 - 0.207\omega j}{1 + 379.404\omega^2} & \frac{-0.181 + 0.271\omega j}{1 + 2.245\omega^2} & \frac{0.999 - 1.823\omega j}{1 + 3.332\omega^2} \end{bmatrix}$$

Table 8
Matrix transfer function for the CCED sequence, using n-pentane as entrainer.

$$\begin{bmatrix} \frac{2.147 - 22.521\omega j}{1 + 110.020\omega^2} & \frac{3.30 \times 10^{-5} - 2.03 \times 10^{-4}\omega j}{1 + 37.722\omega^2} & \frac{-3.01 \times 10^{-6} + 1.87 \times 10^{-5}\omega j}{1 + 38.774\omega^2} \\ \frac{-2.165 + 22.705\omega j}{1 + 110.020\omega^2} & \frac{0.102 - 0.626\omega j}{1 + 37.722\omega^2} & \frac{-0.488 + 3.040\omega j}{1 + 38.774\omega^2} \\ \frac{0.018 - 0.184\omega j}{1 + 110.020\omega^2} & \frac{-0.102 + 0.626\omega j}{1 + 37.722\omega^2} & \frac{0.488 - 3.040\omega j}{1 + 38.774\omega^2} \end{bmatrix}$$

Table 9
Matrix transfer function for the CEDSR sequence, using n-butane as entrainer.

$$\begin{bmatrix} \frac{2.338 - 16.634\omega j}{1 + 50.625\omega^2} & \frac{-1.15 \times 10^{-4} + 4.33 \times 10^{-4}\omega j}{1 + 14.133\omega^2} & \frac{-5.23 \times 10^{-8} + 2.99 \times 10^{-7}\omega j}{1 + 32.581\omega^2} \\ \frac{-2.393 + 17.028\omega j}{1 + 50.625\omega^2} & \frac{0.087 - 0.326\omega j}{1 + 14.133\omega^2} & \frac{-0.035 + 0.019\omega j}{1 + 32.581\omega^2} \\ \frac{0.055 - 0.394\omega j}{1 + 50.625\omega^2} & \frac{-0.086 + 0.325\omega j}{1 + 14.133\omega^2} & \frac{0.035 - 0.198\omega j}{1 + 32.581\omega^2} \end{bmatrix}$$

Table 10
Matrix transfer function for the CEDSR sequence, using n-pentane as entrainer.

$$\begin{bmatrix} \frac{1.341 - 5.731\omega j}{1 + 18.263\omega^2} & \frac{-1.12 \times 10^{-4} + 1.15 \times 10^{-3}\omega j}{1 + 88.471\omega^2} & \frac{-2.83 \times 10^{-6} + 9.19 \times 10^{-6}\omega j}{1 + 10.568\omega^2} \\ \frac{-1.341 + 5.733\omega j}{1 + 18.263\omega^2} & \frac{0.249 - 2.343\omega j}{1 + 88.471\omega^2} & \frac{-0.342 + 1.112\omega j}{1 + 10.568\omega^2} \\ \frac{4.52 \times 10^{-4} - 1.19 \times 10^{-3}\omega j}{1 + 18.263\omega^2} & \frac{-0.249 + 2.342\omega j}{1 + 88.471\omega^2} & \frac{0.342 - 1.112\omega j}{1 + 10.568\omega^2} \end{bmatrix}$$

Table 11
Matrix transfer function for the PCED sequence, using n-butane as entrainer.

$$\begin{bmatrix} \frac{2.141 - 127.509\omega j}{1 + 35417.735\omega^2} & \frac{6.48 \times 10^{-6} - 2.58 \times 10^{-4}\omega j}{1 + 1578.382\omega^2} & \frac{-6.28 \times 10^{-10} + 1.89 \times 10^{-8}\omega j}{1 + 913.464\omega^2} \\ \frac{-2.192 + 130.583\omega j}{1 + 3547.735\omega^2} & \frac{-0.055 + 2.169\omega j}{1 + 1578.382\omega^2} & \frac{-1.693 + 51.165\omega j}{1 + 913.464\omega^2} \\ \frac{0.052 - 3.074\omega j}{1 + 3547.735\omega^2} & \frac{0.055 + 2.168\omega j}{1 + 1578.382\omega^2} & \frac{1.693 - 51.165\omega j}{1 + 913.464\omega^2} \end{bmatrix}$$

Table 12
Matrix transfer function for the PCED sequence, using n-pentane as entrainer.

$$\begin{bmatrix} \frac{1.875 - 110.037\omega j}{1 + 3442.796\omega^2} & \frac{1.46 \times 10^{-4} - 5.82 \times 10^{-3}\omega j}{1 + 1578.736\omega^2} & \frac{-2.11 \times 10^{-8} + 6.37 \times 10^{-7}\omega j}{1 + 914.442\omega^2} \\ \frac{-1.887 + 110.741\omega j}{1 + 3442.796\omega^2} & \frac{-0.109 + 4.321\omega j}{1 + 1578.736\omega^2} & \frac{-1.422 + 42.996\omega j}{1 + 914.442\omega^2} \\ \frac{0.012 - 0.704\omega j}{1 + 3442.796\omega^2} & \frac{0.109 + 4.315\omega j}{1 + 1578.736\omega^2} & \frac{1.422 - 42.199\omega j}{1 + 914.442\omega^2} \end{bmatrix}$$

Table 13
Matrix transfer function for the CCAS sequence.

$$\begin{bmatrix} \frac{2.540 - 1.63 \times 10^{-3}\omega j}{1 + 4.10 \times 10^{-7}\omega^2} & \frac{-3.5 \times 10^{-3} + 1.39 \times 10^{-5}\omega j}{1 + 1.51 \times 10^{-5}\omega^2} \\ \frac{-4.27 \times 10^{-12} + 2.73 \times 10^{-15}\omega j}{1 + 4.10 \times 10^{-7}\omega^2} & \frac{0.010 - 4.04 \times 10^{-5}\omega j}{1 + 1.51 \times 10^{-5}\omega^2} \end{bmatrix}$$

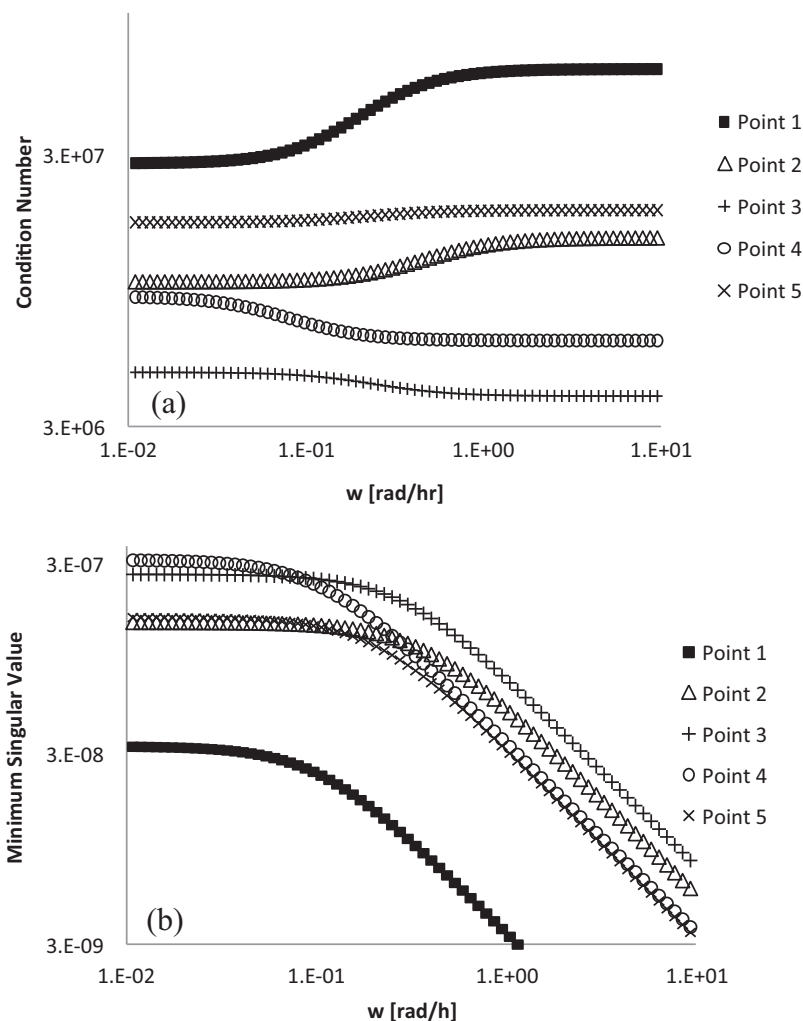


Fig. 12. (a) Condition number, (b) minimum singular values for representative spots inside the "region of analysis" of the sequence CCED n-butane.

8. Conclusions

In this study, the analysis of alternative sequences for the carbon dioxide–ethane mixture is presented. According to the analyzed data, it can be concluded that the alternative thermally coupled sequence (CEDSR) has better generalized performances than the conventional chemical absorption scheme for the carbon dioxide–ethane mixture considered. The principle that among all the alternative arrangements, those having one or more thermal coupling, are characterized by better performances, resulted only partially true because the alternative Petlyuk sequence had a higher value of the TAC together with some problems meeting the purities constraints. Therefore, the type of the mixture (composition and nature) was not entirely suitable for all the thermally coupled distillations systems considered.

Regarding the dynamic behavior for the cryogenic extractive distillation sequence with a side rectifier (CEDSR), the spots (i.e., operating conditions) inside the region of analysis had the best attributes (condition numbers and minimum singular values) compared to the conventional chemical absorption system considered as benchmark process. Only the CEDSR configuration was able to reduce the greenhouse gases emissions reaching high carbon dioxide removals, but also a low thermodynamic efficiency was observed. The methodology used here resulted an effective technique (a pre-selection by using sensitivity analysis and a complementary-study on the Pareto fronts), but at the same time

robust (optimization multi-objective of the designs) for its usage for the separation problem considered.

Acknowledgements

The authors acknowledge for the financial support to this work by Universidad de Guanajuato, CONACYT (Mexico) and for the academic support by University of Southern Denmark, Instituto Tecnológico de Aguascalientes and Università degli Studi di Cagliari.

References

- [1] BP, BP Energy Outlook 2030, January, London, 2012.
- [2] D. Elliot, W.R. Quall, S. Huang, J.J. Chen, R.J. Lee, J. Yao, Y. Zhang, Benefits of integrating NGL extraction and LNG liquefaction technology, in: Proceedings AIChE 2005 Spring National Meeting Conference, 2005, p. 1943.
- [3] S. Freguia, G.T. Rochelle, Modeling of CO₂ capture by aqueous monoethaloamine, AIChE 49 (7) (2003) 1676–1686.
- [4] S. Kim, H.T. Kim, Aspen simulation of CO₂ absorption system with various amine solution, Prepr. Pap. Am. Chem. Soc. Div. Fuel Chem. 49 (2004) 251.
- [5] L.E. Øi, Aspen HYSYS simulation of CO₂ removal by amine absorption from a gas based power plant, in: SIMS2007 Conference, Göteborg, October 30–31st, 2007, pp. 73–81.
- [6] N. Rodriguez, S. Mussati, N. Scenna, Optimization of post-combustion CO₂ process using DEA–MDEA mixtures, Chem. Eng. Res. Des. 89 (2011) 1763–1773.
- [7] B.C. Price, F.L. Gregg, CO₂/EOR: from source to resource, OJ (1983) 116–122, August 22.

- [8] F.W. Schaffert, J.M. Ryan, Koch Process System Inc., Westborough, Mass., Ryan/Holmes technology lands EOR projects, *Oil Gas J.* (1985) 133–136.
- [9] S. Hernández, A. Jiménez, Design of optimal thermally-coupled, distillation systems using a dynamic model, *Trans. IChemE* 74 (1996) 357.
- [10] S. Hernández, A. Jiménez, Controllability analysis of thermally coupled distillation systems, *Ind. Eng. Chem. Res.* 38 (1999) 3957.
- [11] J.G. Segovia-Hernández, S. Hernández, A. Jiménez, A short note about energy efficiency performance of thermally coupled distillation sequences, *Can. J. Chem. Eng.* 84 (1) (2006) 139.
- [12] J.G. Segovia-Hernández, S. Hernández, A. Jiménez, Analysis of dynamic properties of alternative sequences to the Petlyuk column, *Comput. Chem. Eng.* 29 (2005) 1389.
- [13] J.G. Segovia-Hernández, E.A. Hernández-Vargas, J.A. Márquez-Muñoz, Control properties of thermally coupled distillation sequences for different operating conditions, *Comput. Chem. Eng.* 31 (2007) 867.
- [14] S.J. Wang, D.S.H. Wong, Controllability and energy efficiency of a high-purity divided wall column, *Chem. Eng. Sci.* 62 (4) (2007) 1010–1025.
- [15] V.E. Tamayo-Galván, J.G. Segovia-Hernández, S. Hernández, J. Cabrera-Ruiz, J.R. Alcántara-Ávila, Controllability analysis of alternate schemes to complex column arrangements with thermal coupling for the separation of ternary mixtures, *Comput. Chem. Eng.* 32 (12) (2008) 3057–3066.
- [16] M. Errico, G. Tola, B.G. Rong, D. Demurtas, I. Turunen, Energy saving and capital cost evaluation in distillation column sequences with a divided wall column, *Chem. Eng. Res. Des.* 48 (2009) 907–920.
- [17] H. Ling, W.L. Luyben, New control structure for divided-wall columns, *Ind. Eng. Chem. Res.* 48 (2009) 6034.
- [18] H. Ling, W.L. Luyben, Temperature control of the BTX divided-wall column, *Ind. Eng. Chem. Res.* 49 (2010) 189.
- [19] C. Bravo-Bravo, J.G. Segovia-Hernández, C. Gutiérrez-Antonio, A.L. Durán, A. Bonilla-Petriciolet, A. Briones-Ramírez, Extractive dividing wall column: design and optimization, *Ind. Eng. Chem. Res.* 49 (2010) 3672–3688.
- [20] J. He, B. Xu, W. Zhang, C. Zhou, X. Chen, Experimental study and process simulation of n-butyl acetate produced by transesterification in a catalytic distillation column, *Chem. Eng. Proc.* 49 (2010) 132.
- [21] T. Damartzis, P. Seferlis, Optimal design of staged three-phase reactive distillation columns using nonequilibrium and orthogonal collocation models, *Ind. Eng. Chem. Res.* 49 (2010) 3275.
- [22] H. Chan, J.R. Fair, Prediction of point efficiencies in sieve trays: 1. Binary systems, 2. Multicomponent systems, *Ind. Eng. Chem. Proc. Des. Dev.* 23 (1984) 814.
- [23] T.H. Chilton, P.A. Colburn, h-f., *Sg. Chcm.* 26 (1934), 1183.
- [24] F.J. Zuiderweg, Sieve trays: a view on the state of the art, *Chem. Eng. Sci.* 37 (10) (1982) 1441–1464.
- [25] Aspen Technology, Aspen Physical Property System: Physical Property Methods, USA, 2007.
- [26] C.F. Alie, CO₂ Capture with MEA: Integrating the Absorption Process and Steam Cycle of an Existing Coal-Fired Power Plant, Waterloo, Ontario, Canada, 2004 (Master's Thesis).
- [27] X. Xu, Y. Li, Comparison between particle swarm optimization, differential evolution and multi-parents crossover, in: Proceedings of the IEEE International Conference on Computational Intelligence and Security, 2007, pp. 124–127, <http://dx.doi.org/10.1109/cis.2007.37>.
- [28] M.A. Panduco, C.A. Brizuela, A comparison of genetic algorithms particle swarm optimization and the differential evolution method for the design of scannable circular antenna arrays, *Prog. Electromagnet. Res. B* 13 (2009) 171–186.
- [29] S. Sharma, G.P. Rangaiah, Modeling and optimization of a fermentation process integrated with cell recycling and vaporization for multiple objectives, *Ind. Eng. Chem. Res.* 51 (2012) 5542–5551.
- [30] K. Deb, Multi-Objective Optimization Using Evolutionary Algorithms, John Wiley & Sons, New York, 2001.
- [31] R. Turton, R.C. Bailie, W.B. Whiting, J.A. Shaeiwitz, Analysis, Synthesis and Design of Chemical Process, third ed., Prentice Hall, USA, 2009 (appendix A).
- [32] S. Skogestad, M. Morari, The dominant time constant for distillation columns, *Comput. Chem. Eng.* 11 (6) (1987) 607–617.
- [33] V.C. Klema, A.J. Laub, The singular value decomposition: its computation and some applications, *IEEE Trans. Automat. Control* 25 (2) (1980) 164–176.
- [34] J.G. Segovia-Hernández, S. Hernández, V. Rico-Ramírez, A. Jiménez, A comparison of the feedback control behavior between thermally coupled and conventional distillation schemes, *Comput. Chem. Eng.* 28 (2004) 811–819.
- [35] R. Murrieta-Dueñas, R. Gutiérrez-Guerra, J. G. Segovia-Hernández, S. Hernández, Analysis of control properties of intensified distillation sequences: reactive and extractive cases, *Chem. Eng. Res. Des.* 89 (2011) 2215–2227.
- [36] A. Zavala-Guzmán, H. Hernández-Escoto, S. Hernández, J.G. Segovia-Hernández, Conventional proportional – integral (PI) control of dividing wall distillation columns: systematic tuning, *Ind. Eng. Chem. Res.* 51 (2012) 10869–10880.
- [37] J.D. Seader, E.J. Henley, Separation Process Principles, 2nd ed., John Wiley & Sons Inc., USA, 2006, pp. 27–29.
- [38] M.A. Gadalla, Z. Olujic, P.J. Jansens, M. Jobson, R. Smith, Reducing CO₂ emissions and energy consumption of heat-integrated distillation systems, *Environ. Sci. Technol.* 39 (2005) 6860–6870.
- [39] Natural Gas Supply Association, Background, 2010, www.naturalgas.org (accessed 02.05.13).
- [40] F. Lastari, V. Pareek, M. Trebble, M.O. Tade, D. Chinn, N.C. Tsai, K.I. Chan, Extractive distillation for CO₂-ethane azeotrope separation, *Chem. Eng. Process.* (2010), <http://dx.doi.org/10.1016/j.cep.2011.10.001>.
- [41] POGC (Pars Oil and Gas Company), Oil and Gas Processing Plant Design and Operation Training Course Gas Sweetening Processes, 2002, www.pogc.ir (accessed 10.04.13).